

An AKARI Search for Intracluster Dust of Globular Clusters*

Noriyuki MATSUNAGA,^{1,2} Hiroyuki MITO,³ Yoshikazu NAKADA,^{3,4} Hinako FUKUSHI,⁴ Toshihiko TANABÉ,⁴
Yoshifusa ITA,^{5,6} Hideyuki IZUMIURA,⁷ Mikako MATSUURA,^{5,2} Toshiya UETA,⁸ and Issei YAMAMURA⁶

¹*Department of Astronomy, Kyoto University, Kitashirakawa Oiwake-cho, Sakyo-ku, Kyoto, Kyoto 606-8502*
matsunaga@kusastro.kyoto-u.ac.jp

²*Research Fellow of the Japan Society for the Promotion of Science*

³*Kiso Observatory, Institute of Astronomy, School of Science, the University of Tokyo, Mitake, Kiso, Nagano 397-0101*

⁴*Institute of Astronomy, School of Science, the University of Tokyo, 2-21-1 Osawa, Mitaka, Tokyo 181-0015*

⁵*National Astronomical Observatory of Japan, 2-21-1 Osawa, Mitaka, Tokyo 181-8588*

⁶*Institute of Space and Astronautical Science, Japan Aerospace Exploration Agency,*
Yoshinodai 3-1-1, Sagamihara, Kanagawa 229-8510

⁷*Okayama Astrophysical Observatory, National Astronomical Observatory of Japan,*
Kamogata, Asakuchi, Okayama 719-0232

⁸*Department of Physics and Astronomy, University of Denver, Denver, CO 80208, USA*

(Received 2008 May 22; accepted 2008 September 12)

Abstract

We report the observations of 12 globular clusters with the Far-Infrared Surveyor (FIS) on-board AKARI infrared satellite. Our goal is to search for emission from the cold dust within clusters. We detect diffuse emissions toward NGC 6402 and 2808, but the IRAS 100 μm maps show the presence of strong background radiation. They are likely emitted from the galactic cirrus, while we cannot rule out the possible association of a bump of emission with the cluster in the case of NGC 6402. We also detect 28 point-like sources mainly in the WIDE-S images (90 μm). At least several of them are not associated with the clusters but background galaxies based on some external catalogs. We present the spectral energy distributions (SEDs) by combining the near-and-mid infrared data obtained with the Infrared Camera (IRC) if possible. The SEDs suggest that most of the point sources are background galaxies. We find one candidate of the intracluster dust which has no mid-infrared counterpart unlike the other point-like sources, although some features such as its point-like appearance should be explained before we conclude its intracluster origin. For most of the other clusters, we have confirmed the lack of the intracluster dust. We evaluate upper limits of the intracluster dust mass to be between 10^{-5} and $10^{-3} M_{\odot}$ depending on the dust temperature. The lifetime of the intracluster dust inferred from the upper limits is shorter than 5 Myr ($T_d = 70$ K) or 50 Myr (35 K). Such short lifetime indicates some mechanism(s) are at work to remove the intracluster dust. We also discuss its impact on the chemical evolution of globular clusters.

Key words: globular clusters: general — infrared: general — ISM: dust — ISM: evolution — stars: mass loss

1. Introduction

Red giants in globular clusters are known to have low initial masses of about $1 M_{\odot}$ considering their high ages of 10–13 Gyr. Observations revealed that some of the red giants have the mass loss accompanied with dust formation (e.g. Frogel & Elias 1988, Matsunaga et al. 2005). Circumstellar dust has been detected in on-going space missions (*Spitzer Space Telescope*, SST, Boyer et al. 2006, 2008, Origlia et al. 2007; AKARI, Ita et al. 2007). Terminal velocities of the stellar winds from red giants, 10–15 km s^{-1} (McDonald & van Loon 2007), are lower than typical escape velocities from massive globular clusters, $\sim 30 \text{ km s}^{-1}$ (Gnedin et al. 2002). For this reason, one would expect that the released materials are trapped

and accumulated within clusters in the halo region. On the other hand, the intracluster matter is removed by ram pressure when clusters cross the galactic plane. It was expected that gas of the order of $10 M_{\odot}$ exists in a cluster depending on its size and the time since the last passage through the galactic plane (Tayler & Wood 1975).

In spite of the early expectations, most previous attempts failed to detect intracluster matter and placed upper limits which were lower than the expected amounts. The surveys range from the ones of dust to those of different forms of gas (dust, Hopwood et al. 1999; molecular gas, Smith et al. 1995; atomic gas, Faulkner et al. 1991; ionized gas, Knapp et al. 1996; and references therein). Among the challenges to search for intracluster dust, the most secure detection was found in the globular cluster M 15 (Knapp et al. 1995, Evans et al. 2003). Recently, Boyer et al. (2006) confirmed the extended emission of the intracluster dust, which they named IR1a, with SST.

* Based on observations with AKARI, a JAXA project with the participation of ESA.

They also obtained its temperature ($\sim 70\text{K}$) and dust mass ($9 \times 10^{-4} M_{\odot}$) based on the spectral energy distribution (SED). The temperature was found to be higher than that of the interstellar dust (Draine & Anderson 1985; Sodroski et al. 1987). The obtained mass is still 4 times smaller than the expected mass released via the mass loss of red giants. Intracluster gas has been also detected in a couple of cases (e.g. Faulkner et al. 1991, Freire et al. 2001).

The deficiency of the intracluster dust suggests that some mechanism(s) are at work to remove or destroy the dust even in the halo region. The discrepancy between the expected amount of the released dust and the upper limit is larger than ten for some clusters whose intracluster dust has not been detected (Knapp et al. 1995). It remains to be understood what mechanism(s) are efficient to what extent. For example, Lynch & Rossano (1990) proposed sputtering of dust grains by hot halo gas to explain the deficiency. On the other hand, Hopwood et al. (1998, 1999) rejected the sputtering as the mechanism responsible for the removal of the intracluster dust. Penny et al. (1997) presented a list of possible mechanisms. Very recently, Umbreit et al. (2008) demonstrated that stellar collisions can generate the kinetic energy to remove the intracluster dust and gas.

The fate of the released matter within the clusters may have an effect on evolution of globular clusters. Although it was once considered that stars in a globular cluster are chemically homogeneous, more and more studies revealed evidence of inhomogeneity. Readers are referred to Smith et al. (1987), for example, for early investigations mainly about carbon and nitrogen abundances. Recently, the existence of stars enriched in helium have attracted a lot of attention (Norris 2004, Lee et al. 2005). Many authors have argued that those enrichment results from the matter released from intermediate-mass asymptotic giant branch (AGB) stars (e.g. Tsujimoto et al. 2007, Ventura & D’Antona 2008). Suda et al. (2007) proposed that low-mass AGB stars can also play an important role in generating stars with enriched helium contents via intracluster-matter accretion. However, it is not well studied whether the ejecta of AGB stars are actually retained within clusters in the context of dynamics of intracluster gas and dust. The ejecta may disappear before they are used for the generation of enriched stars. The connection to such evolutionary scenarios strengthens the importance to understand how the intracluster matter decreases faster than expected if it is true.

The Far-Infrared Surveyor (FIS; Kawada et al. 2007) on-board AKARI satellite (Murakami et al. 2007) provides us with a new opportunity to investigate the intracluster dust. The FIS can take much deeper images in the far infrared with much higher angular resolution than before. Observations in the far infrared have high sensitivities for the cold dust, $\sim 30\text{K}$. We used the FIS to observe a dozen of globular clusters as a part of the Mission Program to investigate the mass-loss phenomenon in evolved stars in globular clusters and nearby dwarf galaxies (AGBGA; PI, Y. Nakada).

We describe the observation and data reduction in sec-

tion 2. As we will present, we detect a few extended emissions and several point-like sources. Analyses of the extended emissions and the point-like sources are presented in section 3 and 4, respectively. We argue that most of them are not associated with the clusters, while one point-like source remains to be a candidate of the dust within the cluster (section 4.5). In section 5, we present discussions on the mass of the intracluster dust (for both the possible detection and upper limits) and discuss the impact on evolution of globular clusters. Section 6 summarizes this work.

2. Observations and data reduction

2.1. FIS observation

We observed 12 globular clusters by using the AKARI/FIS between 2006 May and 2007 August (table 1). The FIS has four sets of array and filter, named N60, WIDE-S, WIDE-L, and N160. The central wavelengths of their responses are approximately 65, 90, 140, and $160\mu\text{m}$. The formats of the arrays are long and thin, e.g. 3×20 for WIDE-S, and they are designed to make scans along ecliptic meridian. Our data were obtained under the FIS01 slow-scan observational mode with a scan rate of eight arc-seconds per second and a reset interval of two seconds. In this mode, the arrays make two sets of round-trip scans, which produces maps with the fields-of-view of about $20' \times 8'$. The long side of the field is aligned in the direction of ecliptic meridian. Thus, we obtained images around the globular clusters in four filters between 65 and $160\mu\text{m}$.

2.2. Data reduction

The FIS data were first processed with an official data-analysis tool for the slow-scan observation (FIS Slow-Scan Toolkit version 20070914). FITS-format images were created after several procedures such as combination of scanned signals into two-dimensional image and flux calibration. The pixel size of the image was chosen to be $15''$ and $30''$ for $65/90\mu\text{m}$ and $140/160\mu\text{m}$ respectively. Each pixel value was obtained by taking a median of typically five to ten measurements from the round-trip scans. We present the obtained images in the WIDE-S filter in figure 1.

We can find several point sources with expected point spread functions, $\text{FWHM} \sim 40''$ in WIDE-S. Diffuse emissions are also visible in the images of NGC 2808 and NGC 5024. Most of the sources we detected are visible in the WIDE-S images while some of them are also detected in the N60 images. Only a couple of point sources are found in the WIDE-L images, and none in the N160 images. We will focus on the results in the images in two shorter wavelengths unless otherwise mentioned. For further analysis, we used the IRAF¹ as we present in the following sections.

¹ IRAF is distributed by the National Optical Astronomy Observatories, which are operated by the Association of Universities for Research in Astronomy, Inc., under cooperative agreement with the National Science Foundation.

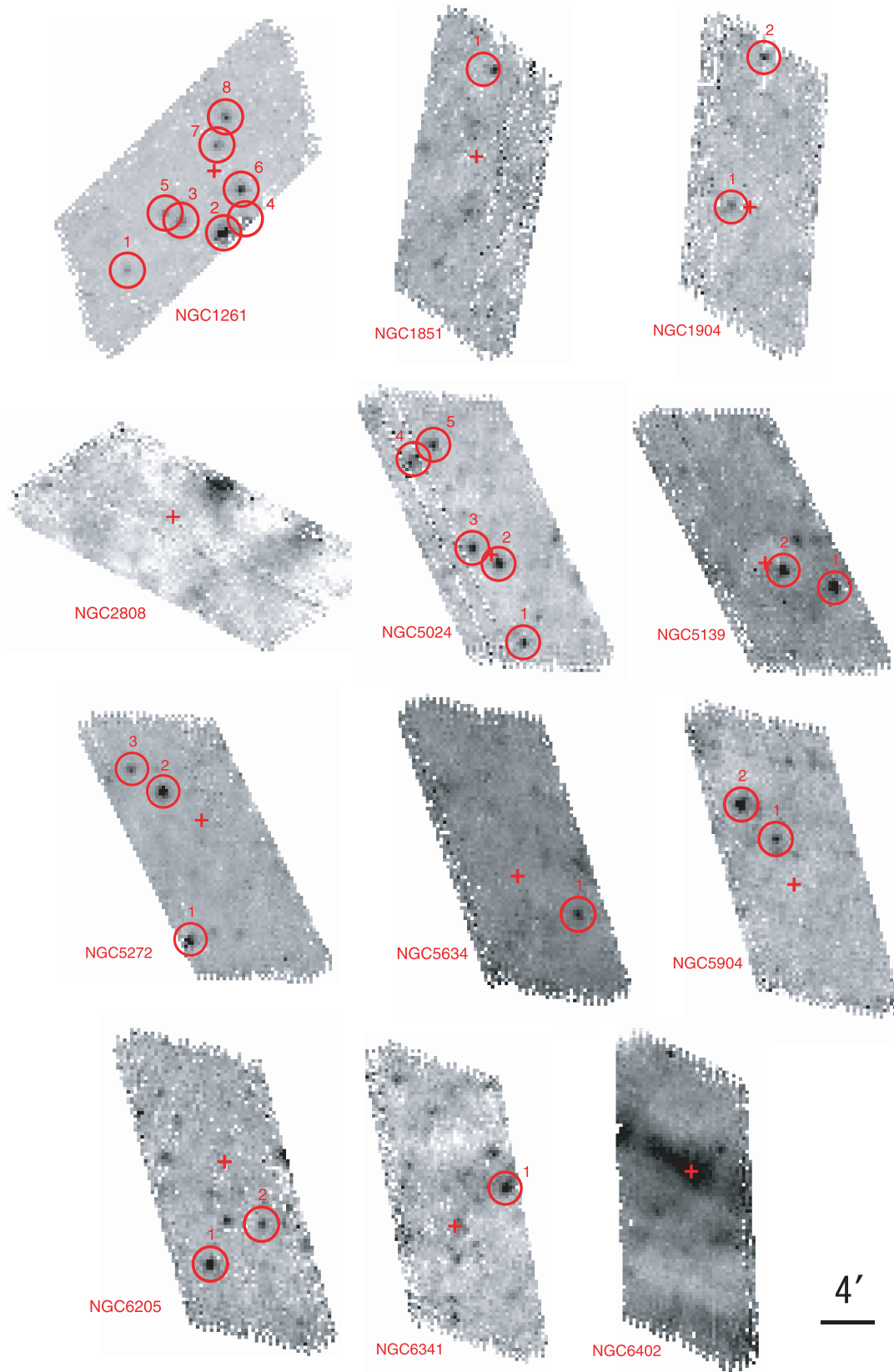


Fig. 1. WIDE-S images of the observed fields. Each image has a field-of-view of about $20' \times 8'$. The long side of the field is aligned in the direction of ecliptic meridian. The north in the equatorial system is up, and the east is left. Cross symbols indicate the centers of the globular clusters. The detected point sources are indicated by circles with the identification numbers.

Table 1. Observation log: the observed globular clusters, their galactic coordinates, observation IDs, and dates. We also list background fluctuations in the obtained images in the unit of MJy/str, σ_{65} for N60, σ_{90} for WIDE-S, σ_{140} for WIDE-L, and σ_{160} for N160.

Name	Alias	RA (°)	Dec (°)	ID	Date	σ_{65}	σ_{90}	σ_{140}	σ_{160}
NGC 1261		48.0637	-55.2169	1700006-001	2006 Dec 29	0.33	0.10	0.41	0.62
NGC 1851		78.5263	-40.0472	1700029-001	2007 Mar 01	0.27	0.09	0.41	0.56
NGC 1904	M 79	81.0442	-24.5242	1700008-001	2006 Sep 10	0.20	0.08	0.36	0.56
NGC 2808		138.0108	-64.8631	1701003-001	2007 Jul 09	0.31	0.15	0.52	0.65
NGC 5024	M 53	198.2304	+18.1692	1700011-001	2006 Dec 31	0.21	0.08	0.34	0.54
NGC 5139	ω Cen	201.6913	-47.4769	1700055-001	2007 Jan 29	0.31	0.13	0.41	0.68
NGC 5272	M 3	205.5467	+28.3756	1701006-001	2007 Jul 03	0.24	0.08	0.34	0.52
NGC 5634		217.4054	-5.9764	1700086-001	2007 Jan 27	0.23	0.09	0.38	0.51
NGC 5904	M 5	229.6408	+2.0828	1700013-001	2007 Feb 06	0.21	0.07	0.35	0.52
NGC 6205	M 13	250.4229	+36.4603	1701019-001	2007 Aug 22	0.26	0.08	0.37	0.56
NGC 6341	M 92	259.2804	+43.1364	1700018-001	2007 Mar 01	0.22	0.08	0.37	0.54
NGC 6402	M 14	264.4004	-3.2458	1700097-001	2006 Sep 16	0.25	0.25	0.90	0.65

2.3. Background fluctuation

In order to estimate background fluctuations of the images, a histogram of pixel values for each image was created and the peak corresponding to the background was fitted with a Gaussian distribution. The standard deviation σ of the fitted Gaussian is adopted as the fluctuation of the background, and listed in table 1. In WIDE-S, for example, most of the images have the fluctuation of about $\sigma \sim 0.08$ [MJy/str]. We find the largest fluctuation in the NGC 6402 image. This is caused by the high background emission of the galactic cirrus (Sodroski et al. 1987). The images for NGC 2808 and NGC 5139 also have slightly larger dispersions. These three clusters have the locations closest to the galactic plane.

3. Analysis of diffuse emissions

3.1. NGC 6402

The image of NGC 6402 (figure 1) reveals extended emission. The cluster center is well projected to within the bump although the bump of emission does not have a sharp peak. In figure 2, we present the IRAS 100 μm map of 1.5 degrees square around NGC 6402. The field of view of the FIS is indicated by a red polygon. Strong large-scale emission clearly exists as a background around this region. In the WIDE-S 90 μm image, for example, the bottom of the background emission is about 15 MJy/str and the emission reaches about 16 MJy/str around the cluster center. The observed bump of emission is comparable to the fluctuation of the large-scale emission. This cluster is the one closest to the galactic plane among our samples ($l = +21.324^\circ$, $b = +14.804^\circ$). There are three possible origins of the bump of emission around NGC 6402. The first one is that the whole emission comes from the interstellar dust (or galactic cirrus) and is not associated with the cluster. Alternatively, the emission can arise from from the intracluster dust within NGC 6402. The last possibility is that the nearby interstellar dust is heated by the cluster.

In order to investigate the nature of the diffuse emission, we performed photometry of the emission around

the cluster. First, we estimated the background emission within an aperture indicated by the dashed circle, which we call sky region, in figure 3. Flux densities are at minimum around the sky region in the FIS images. Then, fluxes above the background level of the sky region were obtained with two different apertures: a circle with the half-mass radius of the cluster around its center ($r < r_h = 1.29'$) and a polygon with an area of 3.43×10^{-6} str as shown in figure 3. The obtained fluxes are listed in table 2. Figure 4 plots the fluxes altogether with the blackbody radiation of 70 K and 25 K. The dust temperature T_d of the bump detected toward NGC 6402 is similar to that of the cirrus in the galactic plane (~ 25 K; Sodroski et al. 1987). We also plot the SED of the stellar and dust components, $T_d = 70$ K, near the core of M 15 reported by Boyer et al. (2006). The SED of the dust component is clearly different from the case of NGC 6402. However, the temperature of a possible intracluster dust cloud can be uncertain because of stochastic effects of the UV flux from hot post-AGB stars, interacting binaries and millisecond pulsars. Millisecond pulsars and X-ray binaries have been found in M 15 (Camilo & Rasio 2005, Dieball et al. 2005, and references therein). There are no such exotic objects found in NGC 6402 although the surveys may not be complete.

In conclusion, the strong background suggests that the bump of emission toward NGC 6402 is likely to be the fluctuation of the galactic cirrus, but we cannot rule out the possible presence of the dust associated with the cluster. It may be interesting to compare the elongation of the bump toward west-northwest with the proper motion of the cluster which is not yet known.

3.2. NGC 2808

The image for NGC 2808 also shows extended emissions though the bumps are separated from the central coordinate of the cluster (figure 1). Figure 5 presents the IRAS 100 μm map of 1.5 degrees square around NGC 2808, which has a large-scale fluctuation as well as NGC 6402. We made photometry on the strongest bump at around the edge with an polygon aperture indicated in figure 6.

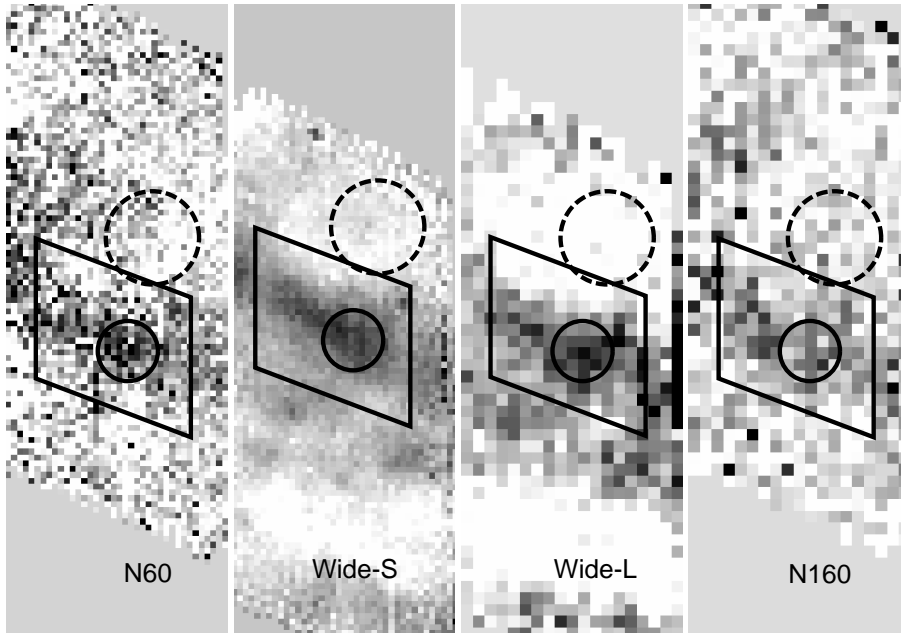


Fig. 3. Four-band images of NGC 6402 and apertures for photometry. The thick circle and the polygon were used to measure the extended emission while the dashed circle was used to estimate the large-scale background emission.

Table 2. Fluxes of the diffuse emissions around NGC 6402 and NGC 2808. The apertures are indicated in figure 3 and 6.

Aperture	Area 10^{-7} str	F_{65} Jy	F_{90} Jy	F_{140} Jy	F_{160} Jy
NGC 6402 (figure 3)					
Filled circle [†]	4.5	0.18	0.31	0.86	0.41
Polygon [†]	34.3	0.66	1.35	3.98	1.75
Dashed circle	10.7	16.4	16.3	29.6	23.9
NGC 2808 (figure 6)					
Polygon [†]	6.2	—	0.31	0.82	—
Dashed circle	10.7	—	9.4	19.1	—

[†] We subtracted the background level estimated in the corresponding dashed circle for each cluster.

The emissions are clear only in the images of WIDE-S and WIDE-L, so that we estimated the fluxes in the two filters and list them in table 2. As we did in the previous section, the background level is evaluated within the dashed circle of two arc-minutes radius indicated in figure 6. The ratio of F_{90}/F_{140} is apparently similar to those obtained for NGC 6402 rather than that of M 15 IR1a. The large-scale fluctuation in the IRAS $100 \mu\text{m}$ map is larger than the bump, $\lesssim 1$ MJy/str, in the WIDE-S image. Therefore, the diffuse emission in direction toward NGC 2808 can be entirely ascribed to the galactic cirrus. The positional difference strongly supports that the emission is not associated with the cluster.

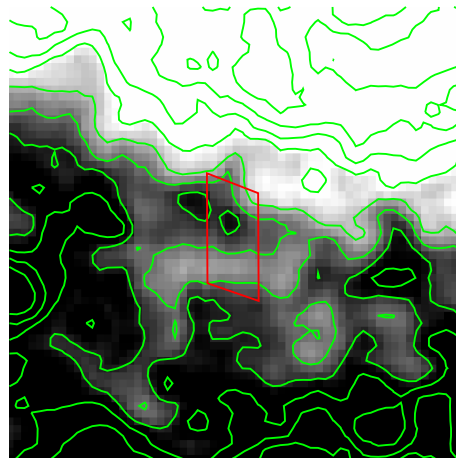


Fig. 2. IRAS $100 \mu\text{m}$ map of 1.5 degrees square around NGC 6402. The north is up and the east is left. The field observed in our AKARI pointed observation in the WIDE-S filter is indicated by a red parallelogram. The contours of the IRAS $100 \mu\text{m}$ flux density are over-plotted at the levels of 15, 16, 17, ..., 25 [MJy/str].

4. Analysis of point-like sources

4.1. Source list

As can be seen in figure 1, several point-like sources are visible in the images. We performed source detections and aperture photometry by using IRAF/APPHOT package. First, the *daofind* task was used to detect the sources with detection limits of 5σ , where σ was chosen to be the background fluctuations listed in table 1. Each candidate was examined by eye in order to exclude spurious pix-

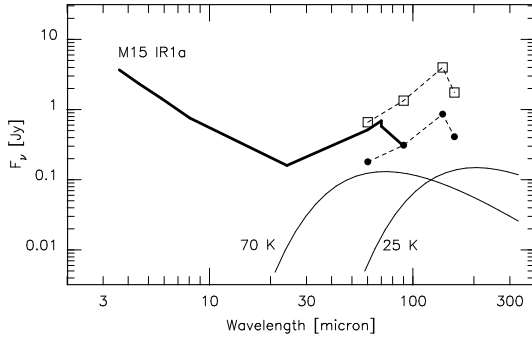


Fig. 4. Spectral energy distribution of the enhancement of the diffuse emission at around NGC 6402. The ones with different apertures are plotted with different symbols (filled circles, a circle aperture within $r \leq r_h$; open squares, a polygon aperture). We also plot the blackbody radiation with 25 K and 70 K (thin curves) and the SED of the stellar and dust components near the core of M 15 reported by Boyer et al. (2006) (thick curve).

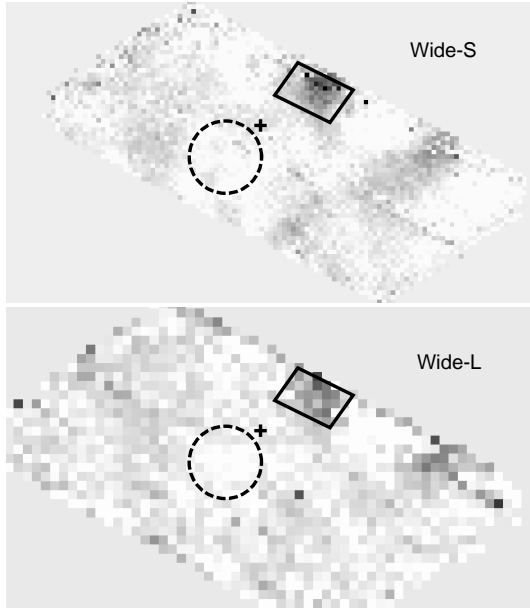


Fig. 6. Two-band images of NGC 2808 and apertures for photometry. The thick polygon was used to measure the extended emission while the dashed circle was used to estimate the large-scale background level.

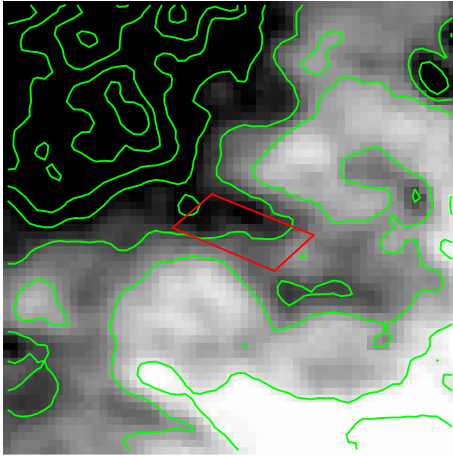


Fig. 5. IRAS 100 μm map of 1.5 degrees square around NGC 2808. The north is up and the east is left. The field observed in our AKARI pointed observation in the WIDE-S filter is indicated by a red parallelogram. The contours of the IRAS 100 μm flux density are overlaid at the levels of 8, 9, 10, ..., 16 [MJy/str].

els. Although some fainter objects seem to be visible, the number of spurious detections get large with a lower detection limit, e.g. 3σ . We decided to set the detection threshold of 5σ . The obtained source list was given to the *phot* task with the apertures ($37.5''$) and sky annuli ($2.'25$ – $3.'25$) listed in the FIS Data User Manual² (Version 1.3; Verdugo et al. 2007). Flux calibration was performed based on the conversion factors, also in the Manual. No color correction was applied.

In table 3, we compile the catalog of the point-like sources. We have detected 28 objects in total. Most of the detections above the 5σ limit are found in WIDE-S images, except N6205 FIS3 detected only in the N60 image which locates out of the WIDE-S field of view. They are indicated by circles in figure 1. The position accuracy is expected to be as good as $\pm 10''$. The dominant source of errors in the obtained fluxes is the uncertainty of the the conversion factors for the calibration (20%, Verdugo et al. 2007).

4.2. Near-to-mid infrared magnitudes

In order to study the natures of the FIS sources, we examined near- and mid-infrared images obtained by using the Infrared Camera (IRC; Onaka et al. 2007) on-board AKARI. Among the 12 clusters in our sample, eight globular clusters were also observed with the IRC, namely NGC 1261, NGC 1851, NGC 2808, NGC 5024, NGC 5139, NGC 5272, NGC 6205, and NGC 6341. The IRC has three channels: NIR (N3 and N4), MIR-S (S7 and S11), and MIR-L (L15 and L24). In the parentheses given are

² The manuals for both FIS and IRC are available at <http://www.ir.isas.jaxa.jp/ASTRO-F/Observation/>

Table 3. Point-like sources found in the direction toward globular clusters. Right Ascensions, Declinations, and flux densities at $90\ \mu\text{m}$ (Wide-S) and $65\ \mu\text{m}$ (N60) are listed. The last column indicates that the source was observed with the IRC (T) or not (F). N5024 FIS2 is given the N flag since it locates within the IRC fields of view but was not detected (see section 4.5).

ID	RA deg	Dec deg	F_{90} mJy	F_{65} mJy	IRC
N1261 FIS1	48.248	-55.336	62	—	F
N1261 FIS2	48.044	-55.291	413	304	T
N1261 FIS3	48.134	-55.276	155	—	T
N1261 FIS4	47.998	-55.275	108	252	T
N1261 FIS5	48.168	-55.267	99	—	T
N1261 FIS6	48.007	-55.239	187	108	T
N1261 FIS7	48.058	-55.185	119	27	T
N1261 FIS8	48.040	-55.152	150	115	T
N1851 FIS1	78.515	-39.936	68	91	F
N1904 FIS1	81.066	-24.524	57	—	F
N1904 FIS2	81.020	-24.332	53	—	F
N5024 FIS1	198.189	18.060	79	79	F
N5024 FIS2	198.221	18.158	114	86	N
N5024 FIS3	198.256	18.177	98	94	T
N5024 FIS4	198.333	18.288	106	—	F
N5024 FIS5	198.307	18.306	86	—	F
N5139 FIS1	201.566	-47.506	195	134	T
N5139 FIS2	201.663	-47.484	132	91	T
N5272 FIS1	205.563	28.221	169	—	F
N5272 FIS2	205.603	28.413	239	301	T
N5272 FIS3	205.650	28.442	89	52	F
N5634 FIS1	217.331	-6.023	66	—	F
N5904 FIS1	229.664	2.139	55	—	F
N5904 FIS2	229.706	2.182	150	101	F
N6205 FIS1	250.444	36.337	99	—	F
N6205 FIS2	250.367	36.385	42	—	F
N6205 FIS3	250.536	36.683	—	143	F
N6341 FIS1	259.192	43.185	95	—	T

the names of the filters we used with the IRC02 observational mode. While NIR and MIR-S channels have the same field of view, MIR-L points to a different field. Thus, two pointing chances are necessary to obtain images of a certain field in all the six filters (once in NIR and MIR-S at the same time, and in MIR-L during another pointing). We obtained the six images for the clusters listed above except NGC 5272 which was only observed in the MIR-L filters.

Raw data were processed with the IRC imaging data pipeline, version 070912 (Lorente et al. 2007). Each IRC image has a field of view of about 10-arcminutes-square around the center of a cluster. With the different shapes of the observed fields, some of the FIS sources in table 3 are not located within the IRC images. For those within the IRC frames, most of the FIS sources have the counterparts which are apparently red, i.e. they are bright in longer wavelength (MIR-L) and faint in shorter wavelength (NIR) compared with numerous normal stars. In a few cases such as N5024 FIS3, there are more than one

NIR objects within the positional accuracy of the FIS source. Nonetheless, it is not difficult to identify a counterpart in the longer wavelength because we can find one-to-one correspondence of the FIS objects to the ones in MIR-L images. It is then possible to select the specific counterparts in the near-infrared images in comparison with the MIR-L images which have higher positional accuracies and resolutions than the FIS images. For N5024 FIS2, we did not find the counterparts even in the MIR-L images.

We used IRAF/DAOPHOT package for photometric measurements, and the fluxes for the FIS counterparts were calibrated into Jy scale, based on the flux conversion factors released on 12 November 2007 (Tanabé, in preparation). They were further transformed into magnitude scale based on the fluxes of the 0-th magnitude: 343, 184, 75.0, 38.3, 16.0, and 8.05 Jy in N3, N4, S7, S11, L15, and L24 filters, respectively. The obtained magnitudes are listed in table 4.

4.3. Spectral energy distributions

Combining the fluxes obtained with the FIS and IRC, we plot the SEDs of the FIS point sources in figure 7. Many of them show a similar character: they have strong emissions in the far infrared and there are bumps at around $10\ \mu\text{m}$. These SEDs are very different from those of any stellar objects. For example, the flux ratio between $100\ \mu\text{m}$ and $25\ \mu\text{m}$ ranges from 20 to more than 100, which is larger than the observed values for post-AGB stars (0.1–4; Volk & Kwok 1989) or planetary nebulae (0.1–10; Pottasch et al. 1984). Overall shape of the SED cannot be attributed to a single component of blackbody radiation either. Even if we assume that there are two components from the cold intracluster dust and one or a group of star(s), their SEDs in the near-to-mid infrared are unlike those of normal stellar components in globular clusters (compare with the SED of M15 IR1a in figure 4).

The SEDs in figure 7 resemble those of galaxies (see Fig. 4 in Sajina et al. 2006, for example). Pearson et al. (2007) calculated the expected AKARI colors for various kinds of galaxies. The flux ratio $F(S7)/F(WIDE-S)$ ranges from 0.001 to 0.1, which agrees with the range of our sample, 0.006–0.85. The bumps at around $10\ \mu\text{m}$ can be attributed to the emission of polycyclic aromatic hydrocarbon (Lee et al. 2007, Sakon et al. 2007).

N5139 FIS1 has a different SED compared with others. This source is identical to the $70\ \mu\text{m}$ source SSTOCEN J132615.23-473024.56 (Source #4) detected by Boyer et al. (2008). As they mentioned, it is potentially affected by blending between a neighboring bright star and a fainter real counterpart of the far-infrared emission. So that, it may be inappropriate to discuss its nature based on the obtained SED.

4.4. Identifications with background galaxies

Here, we further argue that our sources are contaminated with background galaxies. NGC 1261 was included in the FIRBACK survey at $170\ \mu\text{m}$, performed with the ISO (Puget et al. 1999). Four sources we detected in the

Table 4. Near-to-mid infrared magnitudes of the FIS objects. Also listed are coordinates obtained in the IRC images, in S11, whenever available, and differences from the coordinates obtained in the FIS images (Δr).

ID	RA	Dec	Δr	N3	N4	S7	S11	L15	L24
	deg	deg	sec	mag	mag	mag	mag	mag	mag
N1261 FIS2	48.0379	-55.2906	12	12.91	12.35	9.15	8.34	7.53	7.14
N1261 FIS3	48.1286	-55.2747	12	14.30	13.77	10.52	9.56	9.00	8.66
N1261 FIS4	47.9871	-55.2795	29	12.31	11.86	— ^b	9.89	8.21	7.41
N1261 FIS5	48.1629	-55.2657	11	— ^c	— ^c	12.77	10.64	9.93	9.51
N1261 FIS6	47.9992	-55.2373	17	13.82	13.31	11.11	9.35	8.39	8.42
N1261 FIS7	48.0500	-55.1835	16	— ^c	— ^c	— ^c	11.97	11.32	— ^c
N1261 FIS8	48.0321	-55.1489	19	14.01	13.45	10.61	9.43	8.20	7.74
N5024 FIS3	198.2525	+18.1797	14	15.22	15.06	12.25	10.71	8.88	8.41
N5139 FIS1	201.5630	-47.5069	8	9.35	9.34	9.16	8.90	8.33	6.82
N5139 FIS2	201.6596	-47.4846	8	— ^c	— ^c	— ^c	— ^c	— ^c	8.10
N5272 FIS2	205.6028	+28.4147	7	— ^a	— ^a	— ^a	— ^a	7.83	6.26
N6341 FIS1	259.1917	+43.1881	10	14.71	13.48	11.51	10.28	8.49	8.74

^a No image was taken in this filter.

^b The object located out of the field of view.

^c No counterpart was detected in this filter.

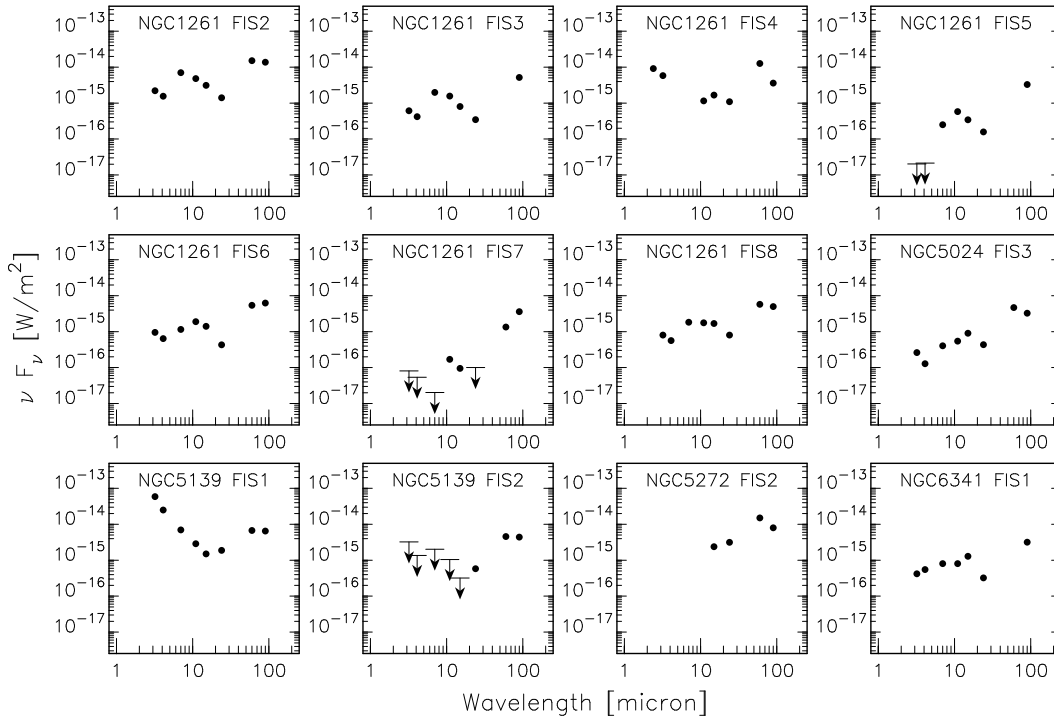


Fig. 7. Spectral energy distributions of the objects observed both in the FIS and the IRC. Arrows are indicated when no counterpart was identified although the image includes the coordinate.

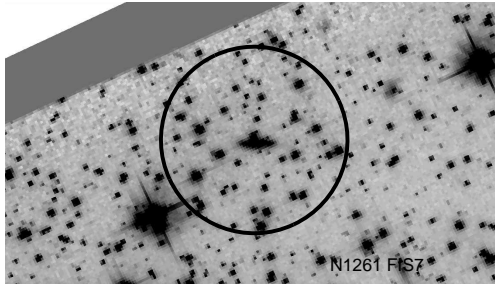


Fig. 8. HST/ACS preview image in F606W around N1261 FIS7, which is indicated by a red circle. The north is up and the east is left, and the field of view is $40'' \times 20''$.

WIDE-S image were already found in their survey, namely, FSM_001 (FIS2), FSM_002 (FIS3), FSM_003 (FIS6), and FSM_007 (FIS8). Patris et al. (2003) made spectroscopic follow-up of the FIRBACK sources and found that the four sources have redshifts between 0.03 and 0.13. We also found galaxies for two other FIS sources with the aid of SIMBAD database,³ MZZ 10046 (emission-line galaxy) for FIS1 and ESO-LV 155-0100 for FIS4. For FIS7, we found a counterpart of galaxy in the preview image of HST/ACS⁴ in both F606W and F814W filters (figure 8). The object is elongated, which suggests that the object is a galaxy. That leaves us only FIS5 that has no hint of background galaxy identification. It is located out of the HST/ACS image. However, its SED looks just like that of the FIS7. It is likely that FIS5 is also a background galaxy. Although the field of NGC 1261 contains the largest number of detected sources among our survey, none of them seems to be associated with the intracluster dust.

For other clusters, there is not much information about the natures of the point-like sources. They do not gather around the cluster center. If they are associated with the clusters, the number detected in each cluster is expected to depend on distance to the cluster because of the limited sensitivity. Such a trend, however, was not found. On the other hand, the number of confusing galactic sources should be dependent on galactic latitude, which is not the case again. We suggest that most of the FIS sources are extragalactic sources, probably background star-forming galaxies based on their similar SEDs to the sources toward NGC1261.

4.5. Remaining candidate of the intracluster dust

We argue that N5024 FIS2 is a candidate of the intracluster dust. First, there is no mid-infrared counterpart found in the IRC images, disclaiming that it is a

³ This research has made use of the SIMBAD database, operated at CDS, Strasbourg, France.
<http://simbad.u-strasbg.fr/simbad/>

⁴ Based on observations made with the NASA/ESA Hubble Space Telescope, obtained from the data archive at the Space Telescope Science Institute. STScI is operated by the Association of Universities for Research in Astronomy, Inc. under NASA contract NAS 5-26555.

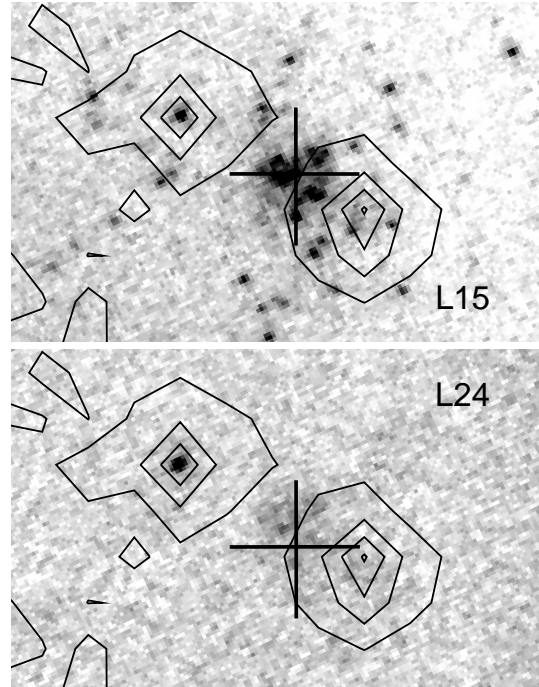


Fig. 9. The close-up figures of the IRC (L15, L24) images of NGC 5024. The central coordinate of the cluster is indicated by the cross. The north is up and the east is left, and the fields-of-view about $6' \times 3.5'$. The contours indicate the flux density in the WIDE-S filter. Among two peaks, the west one corresponds to N5024 FIS2, and the east one to FIS3.

galaxy containing star forming regions within. In figure 9, we present that there is no counterpart of N5024 FIS2, which is in contrast to a neighboring source N5024 FIS3. Although there is a few mid-infrared sources around the peak of N5024 FIS2, none of them is prominent in the L24 image. Compared with the SEDs in figure 7, N5024 FIS2 has smaller mid-infrared emission.

Figure 10 presents the HST/ACS preview images in F606W around the coordinates of the FIS sources, N5024 FIS2 and FIS3. While there is a background galaxy found at the peak of N5024 FIS3, we found no apparent galaxy for the FIS2. We confirmed the same result in the F814W image. This supports the intracluster origin although it is possible that a fainter galaxy or a quasar is associated with them. It is necessary to carry out observations in other wavelength to conclude its nature (see section 5.5).

5. Discussion

5.1. Upper limit of the dust mass from the background fluctuation

In this section, we assess the upper limit of undetected intracluster dust within the half-mass radius r_h based on the background fluctuation. We follow the equation of Lynch & Rossano (1990),

$$f_\nu = 6\sqrt{N}A_p\sigma_\nu, \quad (1)$$

where N is the number of pixels corresponding to the

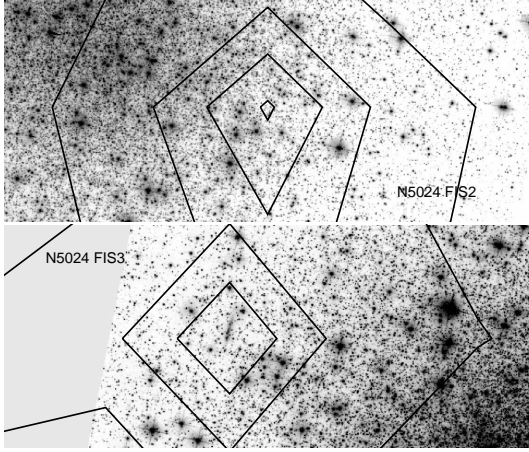


Fig. 10. The Close-up of an HST/ACS preview image in F606W at around N5024 FIS2 and FIS3. The north is up and the east is left, and the fields-of-view are $110'' \times 75''$. The contours indicate the flux density common with those in figure 9.

area, A_p is the area of the pixel, and σ_ν is the standard deviation of the background, to estimate the flux limits (eq. 2). We list the limits of $90 \mu\text{m}$ flux in table 5 with some parameters of the clusters.

According to Boyer et al. (2006), the flux f_ν [mJy] can be converted into the dust mass as,

$$M_d = 4.79 \times 10^{-17} f_\nu \frac{D_{\text{sun}}^2}{\kappa_\nu B_\nu(T_d)} [M_\odot], \quad (2)$$

under the assumption that the dust cloud is optically thin. D_{sun} is the distance in kilo-parsec, κ_ν is the dust absorption coefficient in $\text{cm}^2 \text{g}^{-1}$, $B_\nu(T_d)$ is the Planck function in cgs units, and T_d is the dust temperature. We calculate $\kappa_\nu = 40 \text{ cm}^2 \text{g}^{-1}$ from Ossenkott & Henning (1994) assuming a standard Mathis-Rumpl-Nordsieck dust distribution as Boyer et al. (2006) did. The temperature has a significant effect on the estimate of the dust mass through the Planck function $B_\nu(T_d)$. At $90 \mu\text{m}$, its dependency on the temperature is as $B_{100\text{K}} : B_{70\text{K}} : B_{35\text{K}} = 2.2 : 1 : 0.09$, which directly changes the mass estimate according to equation (2). Angeletti et al. (1982) performed realistic estimates of the temperature of intracluster dust, and obtained temperatures between 35 and 90 K dependent on the assumed chemical composition of dust grain. Here we use two assumed dust temperatures of 35 K and 70 K. The value of 70 K is adopted from the temperature of M 15 IR1a (Boyer et al. 2006). The M_d gets smaller in case of $T_d = 90 \text{ K}$, which accentuates the lack of intracluster dust. The results are listed in table 5.

In figure 11, we plot the estimated upper limits of the intracluster dust against some parameters of the clusters which are taken from Harris (1996) and Gnedin et al. (2002)⁵. We used the Harris catalog available online which was updated in 2003. We also include the mass of the

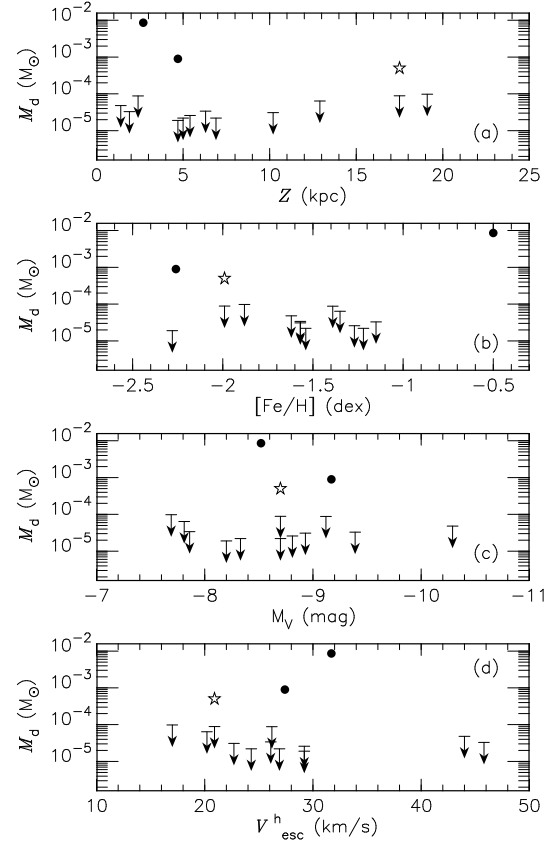


Fig. 11. The mass and upper limits of the intracluster dust plotted against (a) Z -height, (b) metallicity $[\text{Fe}/\text{H}]$, (c) integrated magnitude M_V , and (d) escape velocity at the half-mass radius V_{esc}^h . The y -axis value is based on the assumption of $T_d = 70 \text{ K}$. In case of $T_d = 35 \text{ K}$, all the points shift upward by a factor of 11. The arrows indicate the upper limits obtained in this work, and star symbols indicate the estimated mass of the intracluster-dust candidate N5024 FIS2. Two filled circles indicate M 15 (NGC 7078) and NGC 6356 based on the estimate by Boyer et al. (2006) and Hopwood et al. (1998) respectively.

intracluster-dust candidate, N5024 FIS2 (see section 5.3), and those of the dust clouds in M 15 and NGC 6356 reported in previous studies. No parameter can be an exclusive factor to determine the accumulated mass of the intracluster dust. Although Hopwood et al. (1999) suggested that the metallicity may be an influencing factor based on the fewer samples with shallower observations, the detection of M 15 IR1a disclaims such possibility. It is unclear what parameter(s) determine the amount of the accumulated intracluster dust.

The estimated dust mass of M 15 IRa1 is $(9 \pm 2) \times 10^{-4} M_\odot$, much larger than the upper limits in table 5. Boyer et al. (2006) used a box aperture of $130''.5 \times 130''.5$, which is larger than a circle with $r_h = 1.06'$. Nonetheless, the size of the far-infrared emission of the detected intracluster dust, IR1a, is smaller than the circle so that we can make a direct comparison of the values for IR1a with the upper limits obtained in this work. It is clear

⁵ We used their machine-readable tables on Web: <http://www.physics.mcmaster.ca/Globular.html> <http://www.astro.lsa.umich.edu/%7Eognedin/gc/vesc.dat>

Table 5. Parameters of the observed globular clusters and obtained upper limits. The updated version of Harris (1996) is used to take metallicities $[\text{Fe}/\text{H}]$, integrated magnitudes M_V , distances D_{sun} , and heights Z above or below the galactic plane. Escape velocities at half-mass radii are taken from Gnedin et al. (2002). If available, the velocities V_Z perpendicular to the plane are taken from Dinescu et al. (1999) and Casetti-Dinescu et al. (2007). The 3σ upper limits of the emission $f_{90\mu\text{m}}$ and the mass M_d of the intracluster dust are obtained within the half-mass radii r_h , while τ_d is the upper limit of the lifetime of the dust obtained by equation (5). Two values are listed based on the two assumed dust temperatures, $T_d = 35$ and 70 K, for both M_d and τ_d . The M_d values for N5024 FIS2 (this work) and for M 15 and NGC 6356 (from early papers) are also listed and their lifetimes are obtained in the same manner.

Object	$[\text{Fe}/\text{H}]$ dex	M_V mag	V_{esc}^h km/s	D_{sun} kpc	Z kpc	V_Z km/s	$f_{90\mu\text{m}}$ mJy	M_d		τ_d	
								$10^{-5} M_{\odot}$ 70 K	35 K	10^6 yr 70 K	35 K
NGC1261	-1.35	-7.81	20.2	16.4	12.9	—	16.9	8.8	96	1.9	20
NGC1851	-1.22	-8.33	24.3	12.1	6.9	-109	10.6	3.0	32	0.3	3
NGC1904	-1.57	-7.86	26.1	12.9	6.3	6	14.5	4.6	50	1.6	17
NGC2808	-1.15	-9.39	45.8	9.6	1.9	63	25.8	4.6	50	0.1	2
NGC5024*	-1.99	-8.70	20.9	17.8	17.5	-83	20.1	12.3	133	5.0	55
NGC5139	-1.62	-10.29	44.0	5.3	1.4	-9	122.8	6.7	72	0.3	3
NGC5272	-1.57	-8.93	22.7	10.4	10.2	-154	20.2	4.2	46	0.5	6
NGC5634	-1.88	-7.69	17.0	25.2	19.1	—	11.0	13.5	146	10.9	118
NGC5904	-1.27	-8.81	29.2	7.5	5.4	-222	33.4	3.6	39	0.3	3
NGC6205	-1.54	-8.70	26.9	7.7	5.0	-119	26.9	3.1	34	0.4	5
NGC6341	-2.28	-8.20	29.2	8.2	4.7	35	19.7	2.6	28	3.2	35
NGC6402	-1.39	-9.12	26.2	9.3	2.4	—	72.9	12.2	132	0.9	9
N5024 FIS2	-1.99	-8.70	20.9	17.8	17.5	1.11	114	50	500	10	100
NGC 7078	-2.26	-9.17	27.4	10.3	4.7	1.06	—	90 [†]	—	20	—
NGC 6356	-0.50	-8.52	31.7	15.2	2.7	0.74	—	860 [‡]	—	7	—

*In the event that N5024 FIS2 is not associated with the cluster.

[†]Boyer et al. (2006), [‡]Hopwood et al. (1998).

that the intracluster dust in M 15, which is still smaller than the estimated mass released from red giants (Boyer et al. 2006), is exceptionally large compared with possible intracluster dust in other globular clusters if any. The parameters such as V_{esc}^h and Z -height for at least some of our samples are comparable with those of M 15.

5.2. The lack of intracluster dust

Here we discuss the lack of intracluster dust quantitatively by estimating the lifetime from the expected amount of gas released from red giants. We can calculate the gas amount corresponding to that of the intracluster dust with the dust-to-gas mass ratio ψ . The ratio is considered to be dependent on metallicity. Marshall et al. (2004) concluded that ψ is proportional to the metallicity by comparing OH/IR stars in the solar neighborhood and the large Magellanic Cloud (also see van Loon 2006). It is worthwhile noting uncertainties on ψ especially in the low-metallicity environment. Marshall et al. (2004) found the proportionality between ψ and metallicity based on the objects between $\sim 0.1 Z_{\odot}$ and $\sim 1 Z_{\odot}$. It is not clear if the extrapolation can be applied below $[\text{Fe}/\text{H}] = -1$ dex. Boyer et al. (2006) found more than 20 stars with dusty wind in M15. Although they did not give any estimate on the dust mass-loss rate, some of them have large mid-infrared excesses comparable with the mass-losing stars in the metal-rich cluster 47 Tuc (Origlia et al. 2007). Such dusty mass-loss was not expected in a metal-poor cluster like M 15. If ψ is not so small as expected from the

proportionality, the amount of gas corresponding to the upper limits of dust gets smaller. The ψ value can be changed by non-canonical evolution of stars such as interacting binaries and/or blue stragglers. In the following estimations, we simply assume $\psi = 0.01 \times 10^{[\text{Fe}/\text{H}]}$.

It is possible to evaluate the number of mass-losing stars in a cluster by using the specific evolutionary flux,

$$B \sim 2 \times 10^{-11} \text{ stars yr}^{-1} L_{\odot}^{-1}, \quad (3)$$

which is the number of stars entering or leaving any post-main-sequence stage per year and per solar luminosity of the stellar population (Renzini & Buzzoni 1986). The average dust mass released per year within a cluster can be obtained as,

$$F = \Delta M_d B L_{\text{cl}}, \quad (4)$$

where ΔM_d is the amount of dust to be lost during the post-main-sequence stage and L_{cl} is the total luminosity of the cluster. We assume that each red giant in a cluster loses the gas of $0.2 M_{\odot}$, then ΔM_d is calculated as $0.2\psi M_{\odot} = 2 \times 10^{-3+[\text{Fe}/\text{H}]} M_{\odot}$. We obtain the upper limits of the lifetime of the intracluster dust:

$$\tau_d = \frac{M_d}{F} = \frac{M_d}{\Delta M_d B L_{\text{cl}}/2}. \quad (5)$$

L_{cl} is divided by two because the upper limit M_d has been obtained for the intracluster dust within the half-mass radius. This factor may not be correct if the dust released from stars outside the half-mass radius falls into

the central region of the cluster, in which case the estimated lifetime τ_d gets even smaller.

We list the obtained lifetimes in table 5. Two values are obtained based on the assumed dust temperatures of 35 K and 70 K. The value with $T_d = 35$ K is 11 times larger than the one with $T_d = 70$ K from the ratio of Planck function. In both cases, they are significantly shorter than the typical time interval, $\sim 10^8$ yr, between passages through the galactic plane for most of the clusters. Please note that the τ_d gets even smaller if ψ is larger than the value expected from the proportionality between ψ and $[\text{Fe}/\text{H}]$.

The kinematics information of the clusters suggests that most of the clusters have actually spent a significant time as large as 10^8 yr since the last passage. Here we consider the orbits obtained by Dinescu et al. (1999) and Casetti-Dinescu et al. (2007). The velocity components perpendicular to the galactic plane, i.e. V_z listed in table 5, indicate that five clusters are now approaching to the plane. For NGC 1904 and 5139, V_z almost equals to zero, so that they are in the middle of the passage through the galactic plane. Time since the most recent passages is about the half of the orbital periods or longer for these seven clusters. NGC 1851 and 6341 are still moving away from the plane. NGC 1851 is well separated from the plane by 6.9 kpc. The obtained lifetime, $\tau_d < 3$ Myr, is certainly shorter than the time since its last passage. For NGC 6341, on the other hand, the discrepancy between the obtained lifetime and the time since the last passage is not large to conclude the lack of the intracluster dust in case of $T_d = 35$ K. There are no proper motions available for NGC 1261, 5634, and 6402.

We confirmed that the estimated lifetimes are shorter than the duration in which the intracluster dust can be accumulated since the cluster crossed the galactic plane for at least seven clusters in our sample. The conclusion for NGC 5024 depends on whether N5024 FIS2 belongs to the cluster or not. The short lifetimes indicate that the intracluster dust is not accumulated as was expected and disappears in a short time scale. Thanks to the high sensitivity of the AKARI/FIS, we could conclude the lack of the intracluster dust even with the lower dust temperature of 35 K.

5.3. Estimated mass of the intracluster-dust candidate

We have found a candidate of the intracluster dust, N5024 FIS2. Here, we estimate its mass assuming that it is associated with the cluster. The diffuse emission around NGC 6402 can be associated with the cluster as discussed in section 3.1. However, the clumpy background prevents us from a robust mass estimation, so that we do not include it in quantitative discussions below.

The temperature for N5024 FIS2 cannot be determined well based on our data because of the small coverage of wavelength (only in N60 and WIDE-S) and the limited photometric accuracy ($\pm 20\%$). The flux ratio of $F_{90}/F_{65} = 1.33 \pm 0.4$ corresponds to $T = 55 \pm 15$ [K]. We perform two estimates assuming 70 K and 35 K again. Then, the dust mass of N5024 FIS2 is estimated at $5 \times 10^{-4} M_\odot$ or $5 \times 10^{-3} M_\odot$ for 70 K and 35 K respec-

tively from equation (2). The former value agrees within a factor of 2 with that of M 15 IR1a (Boyer et al. 2006). Under the assumption of the proportionality between ψ and $[\text{Fe}/\text{H}]$, the corresponding gas mass is $5 M_\odot$ (or $50 M_\odot$ if $T_d = 35$ K) so that it is made up of the dust released from a number of stars. The obtained lifetime 10^7 yr (or 10^8 yr) is longer than the upper limits obtained above. If we assume the same dust temperature as the cases of M 15 and NGC 6356, τ_d for N5024 FIS2 is comparable with the lifetimes for the intracluster dust in these clusters.

There remain a few features to be explained if N5024 FIS2 is actually a dust cloud within the cluster. It is offset from the cluster center, i.e. the bottom of the gravitational potential, by $52''$ ($\sim 0.8r_h$). M 15 IR1a is located about $17''$ ($\sim 0.3r_h$) to the west of the cluster core. Boyer et al. (2006) argued that the intracluster dust is short-lived and has not been dynamically relaxed. This can be true for N5024 FIS2 too. Another intriguing feature for our case is that N5024 FIS2 looks like a point source. The estimated mass suggests that a couple of dozen mass-losing stars contributed to N5024 FIS2. The dust clouds released from mass-losing stars aggregated into one blob and it is constrained in a rather small region providing N5024 FIS2 is associated with the cluster. On the other hand, if the dust-to-gas ratio ψ does not follow the proportionality (see section 5.2), the estimated dust mass of N5024 FIS2 does not necessarily exceed the amount released from one object. With $\psi = 0.01$ and $T_d = 70$ K assumed, the estimated amount of the corresponding gas reduces to $0.05 M_\odot$. The size evolution of ejecta from a single AGB star is discussed by Wareing et al. (2007). In the interaction with the interstellar medium, the size of circumstellar shell can be restricted to within a few pc, which is as small as the FWHM ($\sim 40''$) of the FIS at the distance of NGC 5024 (17.8 kpc). It is essential to explain these features in order to conclude the intracluster-dust origin of N5024 FIS2. Theoretical work may be useful to study how the materials released from red giants evolve in the intracluster space and interact with each other.

5.4. Impacts on evolution of globular cluster

As mentioned in the Introduction, intracluster matter may have played an important role in the chemical evolution of globular clusters. Tsujimoto et al. (2007) calculated that a significant amount of the mass released from intermediate-mass AGB stars can be accreted to surrounding stars in NGC 5139 during 2 Gyr. However, it is possible that no significant mass remains to be accreted if the intracluster matter disappears with the short lifetime mentioned above. Of course, it is not dust but gas that should be considered as the source of the mass to be accreted because Tsujimoto et al. (2007) are interested in the enrichment of helium. The fate of the intracluster gas can be rather different from that of the intracluster dust. Previous observations, however, suggest that the intracluster gas is also deficient in globular clusters as mentioned in the introduction. The deficiency was also reported for NGC 5139 (Smith et al. 1990). The conclusion of Tsujimoto et al. (2007) can be altered if the intraclus-

ter gas is removed before it is accreted to the stars within the cluster. Likewise, the fate of the intracluster dust can have an effect on the possible chemical enrichment via the ejecta of evolved stars especially for heavy elements depleted in dust. For example, aluminum abundance pattern has been also explained by the ejecta of AGB stars (Denissenkov et al. 1998, Ventura & D'Antona 2008).

In any case, it is of interest to investigate the evolution, destruction, and/or removal of the intracluster gas and dust in the context of their effects on the evolution of globular clusters. It is possible that globular clusters were embedded in dark matter halos once in the early universe and the intracluster-matter evolution was different from that in current clusters (Bekki 2006). Nonetheless, observation of current ones can provide important constraints to be compared with detailed modeling.

5.5. Future prospects

Besides pointed observations as those presented here, AKARI accomplished the All-Sky Survey. The expected sensitivity is lower than those of the pointed observations. The 5σ detection limit in the WIDE-S filter is 0.55 Jy for a point source (Kawada et al. 2007). Nonetheless, it is similar to that in previous observations made with the ISO which resulted in a couple of detections (Hopwood et al. 1998; Evans et al. 2003). The All-Sky Survey data will enable us to search for the intracluster dust in all the globular clusters with a reasonable detection limit.

On the other hand, with the high sensitivity of the FIS pointed observations, a significant number of background galaxies appear above the detection limit. In the future surveys, it can become a problem to discriminate the intracluster dust from the background galaxies unless they are more extended than expected for galaxies. A potentially useful method is to combine the radio observation for the sources. It is well known that the FIR-radio correlation holds for various kinds of galaxies (Dickey & Salpeter 1984). Oyabu et al. (2005) explored the correlation for the far-infrared sources in the Lockman Hole region based on the ISO's survey (90 and 170 μm) and 1.4 GHz observations with Very large Array (VLA). We can obtain $\log(F_{90\mu\text{m}}/F_{1.4\text{GHz}}) \sim 2.8$ based on their data. This value increases to about 6.2 if we consider the blackbody radiation of 70 K. Therefore, the radio flux clearly discriminates between the intracluster dust and background galaxies assuming that intracluster dust has a temperature of 70 K as M 15 IR1a. As for the source we detected, $F_{90\mu\text{m}}$ of about 100 mJy predicts $F_{1.4\text{GHz}} \sim 700 \mu\text{Jy}$ for the galaxies and ~ 60 nano-Jy for the blackbody radiation of 70 K. Though the expected $F_{1.4\text{GHz}}$ value is lower than the detection limits of the wide-field survey catalog currently available even for the case of galaxies, deep follow-up observations may tell which is the case.

6. Summary

We obtained far-infrared images for 12 globular clusters with the AKARI/FIS, which allowed us to do deep surveys of the cold intracluster dust. While we found one candi-

date of the intracluster dust, we confirmed the paucity of such dust in most clusters.

In the FIS images, we detected extended emissions toward two clusters, namely NGC 2808 and NGC 6402. They are separated from the galactic plane by less than 15 degrees, and large-scale emission of the galactic cirrus is dominant in their fields. We suggest that the detected bumps of emission are merely fluctuations of the background emission. In case of NGC 2808, the emission is largely away from the cluster center, while the bump coincides with the center of NGC 6402. We cannot rule out the possible dust component associated with NGC 6402.

On the other hand, we detected 28 point-like sources, but concluded that most of them are background galaxies. For those with the near-to-mid infrared data by the AKARI/IRC, the obtained SEDs resemble those of galaxies. We found one source, N5024 FIS2, without any clear counterpart in the mid infrared. There is no galaxy found in the HST/ACS image at around the coordinate. It is a possible candidate of the intracluster dust. If so and the temperature of 70 K is assumed, the dust mass is estimated at $5 \times 10^{-4} M_{\odot}$. However, some intriguing features such as the point-like appearance remain to be explained if N5024 FIS2 actually belongs to the cluster. Besides the candidate, our results give upper limits of $2-9 \times 10^{-5} M_{\odot}$ within the half-mass radii of the 12 clusters from the background fluctuation.

Some mechanism(s) are clearly efficient to remove the intracluster dust in most clusters, if not all. The lifetime of the intracluster dust is as short as 10^{5-6} yr. On the other hand, we found that the intracluster dust detected in M 15 and NGC 6356 is exceptionally large compared with other clusters. Our result strengthens the mystery of the lack of the intracluster dust. It urges us to study physical processes which determine the fate of the intracluster dust. Together with that of the intracluster gas, it has a potential to affect the evolution of globular clusters.

We acknowledge the anonymous referee whose helpful comments gave us a chance to improve the paper. We thank Shinki Oyabu for his suggestions about the usefulness of radio follow-up observation. We are grateful to Iain McDonald for helpful comments based on his analysis on the Spitzer Space Telescope data.

References

- Angeletti, L., Blanco, A., Bussoletti, E., Capuzzo-Dolcetta, R., & Giannone, P. 1982, MNRAS, 199, 441
- Bekki, K., 2006, MNRAS, 367, L24
- Boyer, M. L., Woodward, C. E., van Loon, J. Th., Gordon, K. D., Evans, A., Gehrz, R. D., Helton, A., & Polomski, E. F. 2006, AJ, 132, 1415
- Boyer, M. L., McDonald, I., van Loon, J. Th., Woodward, C. E., Gehrz, R. D., Evans, A., & Dupree, A. K. 2008, AJ, 135, 1395
- Camilo, F., Rasio, F. A., 2005, ASPC, 328, 147
- Casetti-Dinescu, D. I., Girard, T. M., Herrera, D., van Altena, W. F., Lopez, C. E., & Castillo, D. J., AJ, 134, 195

- Denissenkov, P. A., Da Costa, G. S., Norris, J. E., & Weiss, A. 1998, *A&A*, 333, 926
- Dickey, J. M., & Salpeter, E. E. 1984, *ApJ*, 284, 461
- Dieball, A., Knigge, C., Zurek, D. R., Shara, M. M., Long, K. S., Charles, P. A., Hannikainen, D. C., van Zyl, L. 2005, *ApJ*, 634, L105
- Dinescu, D. I., Girard, T. M., & van Altena, W. F. 1999, *AJ*, 117, 1792
- Draine, B. T., & Anderson, N. 1985, *ApJ*, 292, 494
- Evans, A., Stickel, M., van Loon, J. Th., Eyres, S. P. S., Hopwood, M. E. L., & Penny, A. J. 2003, *A&A*, 408, L9
- Faulkner, D. J., Scott, T. R., Wood, P. R., & Wright, A. E. 1991, *ApJ*, 374, L45
- Freire, P. C., Kramer, M., Lyne, A. G., Camilo, F., Manchester, R. N., & D'Amico, N. 2001, *ApJ*, 557, L105
- Frogel, J. A., & Elias, J. H. 1988, *ApJ*, 324, 823
- Harris, W. E. 1996, *AJ*, 112, 1487
- Hopwood, M. E. L., Evans, A., Penny, A., & Eyres, S. P. S. 1998, *MNRAS*, 301, L30
- Hopwood, M. E. L., Eyres, S. P. S., Evans, A., Penny, A., & Odenkirchen, M. 1999, *A&A*, 350, 49
- Ita, Y., et al. 2007, *PASJ*, 59, S437
- Kawada, M., et al. 2007, *PASJ*, 59, S389
- Knapp, G. R., Gunn, J. E., & Connolly, A. J. 1995, *ApJ*, 448, 195
- Knapp, G. R., Gunn, J. E., Bowers, P. F., & Vasquez Poritz, J. F. 1996, *ApJ*, 462, 231
- Lee, Y.-W., et al. 2005, *ApJ*, 621, L57
- Lee, H.-M., et al. 2007, *PASJ*, 59, S529
- Lorente, R., Onaka, T., Ita, Y., Ohyama, Y., Tanabé, T., & Pearson, C. 2007, *AKARI IRC Data User Manual Version 1.3*
- Lynch, D. K., & Rossano, G. S. 1990, *AJ*, 100, 719
- Marshall et al. 2004, *MNRAS*, 355, 1348
- Matsunaga, N., Deguchi, S., Ita, Y., Tanabé, T., & Nakada, Y. 2005, *PASJ*, 57, L1
- McDonald, I., & van Loon, J. Th. 2007, *A&A*, 476, 1261
- Murakami, H., et al. 2007, *PASJ*, 59, S369
- Norris, J. E. 2004, *ApJ*, 612, L25
- Gnedin, O. Y., Zhao, H.-S., Pringle, J. E., Fall, M. S., Lovio, M., & Meylan G. 2002, *ApJ*, 568, L23
- Onaka, T., et al. 2007 *PASJ*, 59, S401
- Origlia, L., Rood, R. T., Fabbri, S., Ferraro, F. R., Fusi Pecci, F., & Rich, R. M., 2007, *ApJ*, 667, L85
- Ossenkopf, V., & Henning, Th., 1994, *A&A*, 291, 943
- Oyabu, S., et al. 2005, *AJ*, 130, 2019
- Patris, J., Dennefeld, M., Lagache, G., & Dole, H. 2003, *A&A*, 412, 349
- Pearson, C. P., et al. 2007, *Advances in Space Research*, 40, 605
- Penny, A. J., Evans, A., & Odenkirchen, M. 1997, *A&A*, 317, 694
- Piotto, G., et al. 2007, *ApJ*, 661, L53
- Pottasch, S. R. et al. 1984, *A&A*, 138, 10
- Puget, J. L, et al. 1999, *A&A*, 345, 29
- Renzini, A., & Buzzoni 1986, in *Spectral Evolution of Galaxies*, ed. C. Chiosi & A. Renzini (Dordrecht: Reidel), 135
- Sajina, A., Scott, D., Dennefeld, M., Dole, H., Lacy, M., & Lagache, G. 2006, *MNRAS*, 369, 939
- Sakon, I., et al. 2007, *PASJ*, 59, S483
- Smith, G. H. 1987, *PASP*, 99, 67
- Smith, G. H., Wood, P. R., Faulkner, D. J.; Wright, A. E. 1990, *ApJ*, 353, 168
- Smith, G. H., Woodsworth, A. W., & Hesser, J. E. 1995 *MNRAS*, 273, 632
- Sodroski, T. J., Dwek, E., Hauser, M. G., & Kerr, F. J. 1987, *ApJ*, 322, 101
- Suda, T., Tsujimoto, T., Shigeyama, T., & Fujimoto, M. Y. 2007, *PASJ*, 671, L129
- Tayler, R. J., & Wood, P. R. 1975, *MNRAS*, 171, 467
- Tsujimoto, T., Shigeyama, T., & Suda, T. 2007, *ApJ*, 654, L139
- Umbreit, S., Chatterjee, S., & Rasio, F. A. 2008, *ApJ*, in press (arXiv:0805.2358)
- van Loon, J. Th. 2006, *ASPC*, 353, 211
- Ventura, P., & D'Antona, F. 2008, *A&A*, 479, 805
- Verdugo, E., Yamamura, I., & Pearson, C. P. 2007, *AKARI FIS Data User Manual Version 1.3*
- Volk, K. M., & Kwok, S. 1989, *ApJ*, 342, 345
- Wareing, C. J., Zijlstra, A. A., & O'Brien, T. J. 2007, *MNRAS*, 382, 1233